

Heat transfer analysis of phase change process in a finned-tube thermal energy storage system using artificial neural network

Kemal Ermis^{a,c,1}, Aytunc Ereğ^b, Ibrahim Dincer^{c,*}

^a Department of Mechanical Education, Sakarya University, Sakarya, 54187, Turkey

^b Department of Mechanical Engineering, Dokuz Eylül University, Bornova, 35100 Izmir, Turkey

^c Faculty of Engineering and Applied Science, University of Ontario Institute of Technology (UOIT),
2000 Simcoe Street North, Oshawa, Ont., Canada L1H 7K4

Received 15 April 2006

Available online 8 March 2007

Abstract

In this study, a feed-forward back-propagation artificial neural network (ANN) algorithm is proposed for heat transfer analysis of phase change process in a finned-tube, latent heat thermal energy storage system. Heat storage through phase change material (PCM) around the finned tube is experimentally studied. A numerical study is performed to investigate the effect of fin and flow parameter by the solving governing equations for the heat transfer fluid, pipe wall and phase change material. Learning process is applied to correlate the total heat stored in different fin types of tubes, various Reynolds numbers and different inlet temperatures. A number of hidden numbers of ANN are trained for the best output prediction of the heat storage. The predicted total heat storage values obtained by an ANN model with extensive sets of non-training experimental data are then compared with experimental measurements and numerical results. The trained ANN model with an absolute mean relative error of 5.58% shows good performance to predict the total amount of heat stored. The ANN results are found to be more accurate than the numerical model results. The present study using ANN approach for heat transfer analysis in phase change heat storage process appears to be significant for practical thermal energy storage applications.

© 2007 Elsevier Ltd. All rights reserved.

Keywords: Heat transfer rate; Finned tube; Thermal energy storage; Artificial neural networks; Numerical simulation; Phase change material

1. Introduction

Thermal energy storage (TES) is considered to be one of the most important energy technologies, and recently, increasing attention has been paid to utilizing TES in a variety of thermal engineering applications ranging from heating to cooling (including air conditioning) processes [1]. TES systems are now popular in many countries, particularly in Canada, the United States, and Europe. Because these are the most efficient methods to avoid costly energy price and to reduce summer-time peak load electricity

demand. The increased cooling demand results in peak electrical power demand during the hottest summer days. TES systems not only shift cooling energy to use at non-peak times, but also reduce energy consumption, depending on site-specific design, notably where chillers can be operated at full load during the night. Dincer and Rosen [2] explained energetic, environmental and economic aspects of thermal energy storage systems for cooling capacity and found some of the advantages of utilizing TES such as reduced energy cost, consumption, equipment size and pollutant emissions, also increased flexibility of operation, efficiency and effectiveness of equipment utilization (for details, see [3]).

Many researchers have focused on storing energy through the phase-change material due to their relatively low volume requirement and narrow band of temperature variation. A few studies related to the heat transfer through

* Corresponding author. Tel.: +1 905 721 3111; fax: +1 905 721 3140.

E-mail addresses: Kemal.Ermis@uoit.ca (K. Ermis), aytunc.erek@deu.edu.tr (A. Ereğ), Ibrahim.Dincer@uoit.ca (I. Dincer).

¹ Post Doctoral Fellow at UOIT.

Nomenclature

a_i	experimental value	<i>Greek symbols</i>	
ANN	artificial neural network	θ	external threshold, or dimensionless temperature, $(T - T_m)/(T_m - T_{in})$
AMRE	absolute mean relative error	θ_j	threshold between the input and hidden layers
c, c_p	specific heat ($\text{J kg}^{-1} \text{K}^{-1}$)	$\delta\theta_m$	$\delta T/(T_m - T_{in})$
C^0	heat capacity ($\text{J m}^{-3} \text{K}^{-1}$), $c^* \rho$	H	latent heat of PCM (J kg^{-1})
C	$C^0/(c_1 \cdot \rho_1)$	$f()$	logistic sigmoid activation function
C_{sl}	c_s/c_l	$f_h()$	logistic sigmoid activation function from input layer to hidden layer
D	inside diameter of the circular pipe (m)	λ	variable which controls the slope of the sigmoid functional
d_k	target activation of output layer	θ_k	threshold connecting the hidden and output layers
H	enthalpy (J kg^{-1})	$f_k()$	logistic sigmoid activation function from hidden layer to output layer
HTF	heat transfer fluid	f'_k	local slope of the node activation function for output nodes
h	vector of hidden-layer neurons	δ_k	vector of errors for each output neuron
k	thermal conductivity ($\text{W m}^{-1} \text{K}^{-1}$)	δ_j	vector of errors for each hidden layer neuron
K	dimensionless thermal conductivity (k/k_1)	f'_h	local slope of the node activation function for hidden nodes
K_{sl}	k_s/k_l	α	learning rate, or thermal diffusivity ($\text{m}^2 \text{s}^{-1}$)
L	length of pipe (m)	μ	dynamic viscosity (N s m^{-2})
\dot{m}	mass flow rate (kg s^{-1})	ρ	density (kg m^{-3})
n	number of the data	τ	dimensionless time, $\alpha_f \cdot t/D^2$
Nu	Nusselt number	η	momentum factor
PCM	phase change material	ν	kinematic viscosity (m s^{-1})
R^2	absolute fraction of variance	<i>Subscripts</i>	
STD	standard deviation	f	transfer fluid, or fin
TES	thermal energy storage	h	hidden layer
Pe_f	fluid Peclet number, $Re_f \cdot Pr_f$	i	input node, or initial condition
Pr_f	fluid Prandtl number, ν_f/α_f	inf	outside of the thermal storage tank
Q	dimensionless total stored energy	in	inlet
r	radial coordinate (m)	j	hidden layer node
R	dimensionless radial direction, r/D or solidification front	k	output layer node
Re_f	fluid Reynolds number, $\frac{4\dot{m}}{\pi D \mu_f}$	l	liquid PCM
S^0	source term	n	number of the data
S	dimensionless source term, $S^0/\rho_1 c_1 (T_m^0 - T_{in}^0)$	m	mushy phase
Ste	Stefan number	s	solid PCM
t	time period, or fin thickness (m)	w	container wall or surface
T	temperature (K)		
w	fin spacing (m)		
w_{ij}	weights connecting the i th input node to the j th hidden layer node		
w_{kj}	weights connecting the j th hidden layer node to the k th output layer		
X	dimensionless axial direction, x/D		
x	multiple inputs, or axial coordinate (m)		
y	output		
y_i	prediction value		

solidification or melting have been published in the last decade. A theoretical model of the shell-and-tube type unit has been reported by [4]. Cao and Faghri [5,6] modeled a similar problem at which both the heat charging and the recovery processes were performed by the circulating fluid for the shell wall of the unit assumed to be adiabatic. Bellecci and Conti solved the problem of storing energy in a shell-and-tube type unit by using the enthalpy model. Cao and Faghri

[6] studied the latent heat energy storage systems for both annular and countercurrent flows and numerically determined the countercurrent flow was an efficient way to absorb heat energy. Many theoretical and experimental studies have been undertaken by various researchers, e.g., [7–12] to investigate the solidification of phase change material around finned tube, considering steady and unsteady effects, geometry, convection effects, etc.

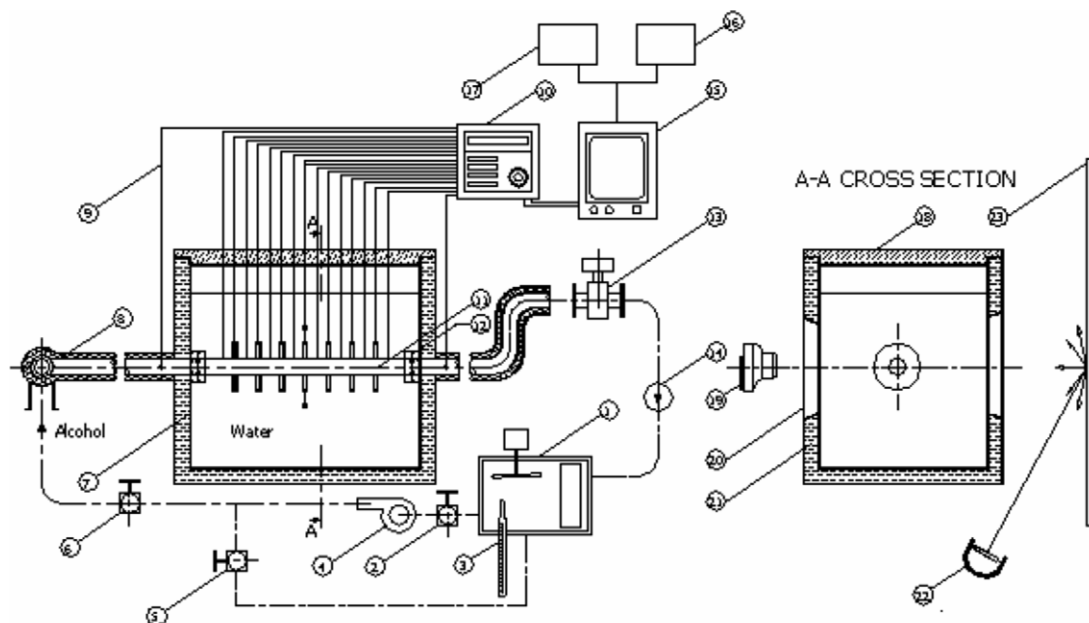
This study focuses on prediction of total thermal energy stored in latent heat thermal storage systems by using experimental data and artificial neural network (ANN) model. ANNs are non-linear mapping systems whose structures are based on principles inspired by the biological nervous systems of humans. An ANN consists of a large number of simple processors linked by weighted connections. By analogy, the processing units are called neurons. Neural networks provide a fundamentally different approach from the numerical solution methods to forecast the future project. This technique has been applied in many disciplines of science and has produced preliminary results in many areas of modeling a system, e.g., [13–19].

Although various analytical and numerical heat transfer models have been employed for thermal modeling of latent heat storage systems, ANN methods have not yet been applied to such systems for thermal modeling. This is the motive behind the present work which aims to study heat transfer aspects during phase change process in a finned tube latent heat storage system and compare its results with some numerical calculations and experimental data.

2. Experimental procedure

The experimental data obtained from an experimental test unit as shown in Fig. 1 is used for analysis. The experimental unit basically consists of the flow system, heat transfer test section and temperature measurement system. Its heat transfer test section consists of an energy storage

tank, having dimensions of 420 mm × 570 mm × 500 mm (width × length × height), finned tube and phase change material (e.g., water) around this tube. To visualize the solidification fronts around the finned tube, a digital camera is used, and the data are then transmitted to a PC. The base of the tank is supported with 50 mm thick Styrofoam layer and, the side walls and the top wall are covered with 3 cm thick Styrofoam layer for insulating the tank to obstruct heat losses. The finned tubes are made of a solid bronze cylinder (87.2% Cu, 6.57% Sn, 4.13% Zn and 1.97% Pb). All tubes have the same total length of 570 mm (with a finned length of 440 mm), a fin thickness of 3 mm, and inner and outer tube radii of 10 mm and 15 mm, respectively. The tube dimensions are listed in Table 1. A reservoir for the heat transfer fluid, constant temperature circulating bath, variable speed pump, flow meter and the hydrodynamic entry section are the essential parts of the flow system. The hydrodynamic entry section length is chosen long enough as ~240 diameter, 6500 mm in order to provide fully developed flow conditions for the heat transfer fluid at the inlet of the energy storage unit. Ethyl-alcohol (CH₃-CH₂OH) is used as the heat transfer fluid to assure liquid behavior for such a low temperature range. A data logger is employed for temperature measurements. The thermocouples are embedded into midsections of the fin tip and the base sensed the surface temperature. The pure water is used as the test PCM and initially cooled down to the temperature of 0.3 °C to be pumped into the insulated storage tank. The experimental data are taken



1: Constant temperature bath; 2: main valve; 3: thermometer; 4: alcohol circulation pump; 5: recirculation valve; 6: flow adjustment valve; 7: energy storage tank; 8: connecting pipe; 9: thermocouple extension wires; 10: data logger; 11: finned tube; 12: fittings; 13: flow meter; 14: check valve; 15: PC computer; 16: monitor; 17: disc drive; 18: tank top cover; 19: digital camera; 20 plexiglass view window; 21: insulation; 22: light source; 23: white screen

Fig. 1. The experimental test system [12].

Table 1
The dimensions of the tubes used in the experiments

Tube type	Number of fins	Fin diameter (mm)	Fin spaces (mm)	Heat transfer area (m ²)
1 (bare tube)	–	–	–	0.094248
2	7	54	65.0	0.164961
3	7	64	65.0	0.193621
4	11	54	40.0	0.206030
5	11	64	40.0	0.251327
6	15	54	27.5	0.250517
7	15	64	27.5	0.313855

at three different inlet temperatures of $-10\text{ }^{\circ}\text{C}$, $-15\text{ }^{\circ}\text{C}$ and $-20\text{ }^{\circ}\text{C}$ and six different Reynolds number varies between 500 and 7000 flow rates of conditions. Thus, a total of 45 experimental runs are carried out. More details of experimental procedure can be found in [12].

3. Numerical model

A schematic representation of the physical model for a finned-tube heat storage unit for analysis is shown in Fig. 2. The PCM fills the annular space, around the finned tube, of inner radius r_o and outer radius r_{inf} , while the heat transfer flows inside the tube. The tube wall has inner and outer radii of r_i and r_o . The outside wall of the energy storage unit is insulated. The thermophysical properties of the PCM, tube wall and heat transfer fluid (HTF) are independent of temperature, but the properties of the PCM can be different into the solid and liquid phases. Initially, the system is set to a temperature of T_i higher than T_m . The HTF (at a temperature of T_{in}) less than T_m flows into the finned tube to form solidification around the finned tube. To model this process, the system is divided into following three subsections: (i) tube flow of heat transfer fluid, (ii) the finned tube, and (iii) the region filled by PCM.

The following dimensionless variables and groups are introduced here for analysis:

$$R = \frac{r}{D}, \quad X = \frac{x}{D}, \quad \tau = \frac{\alpha_f \cdot t}{D^2}, \quad \theta = \frac{T - T_m}{T_m - T_{in}},$$

$$\delta\theta_m = \frac{\delta T_m}{T_m - T_{in}},$$

$$Re = \frac{4\dot{m}}{\pi D \mu_f}, \quad Pr_f = \frac{\gamma_f}{\alpha_f}, \quad Pe_f = Re_f \cdot Pr_f,$$

$$Ste = \frac{c_{pl} \cdot (T_m - R_{in})}{\Delta H},$$

$$C = \frac{C^0}{\rho_1 c_1}, \quad S = \frac{S^0}{\rho_1 c_1 \cdot (T_m - T_{in})}, \quad K = \frac{k}{k_1}.$$

Assuming that axial conduction is negligible and that the fully developed conditions exist at the tube inlet, the dimensionless energy equation of the heat transfer fluid can be expressed as

$$\frac{\partial \theta_b}{\partial \tau} = 4Nu_b(\theta_w - \theta_b) - Re_f Pr_f \frac{\partial \theta}{\partial X}. \quad (1)$$

The quasi-steady assumption is applied to the convection heat transfer inside the tube. Transient convection is considered inside the tube as a series of steady state forced convection problems. For laminar flow, the local Nusselt number can be obtained by an analytical method with arbitrary varying temperature at the tube wall as described by [20,21]:

$$(Nu_b)_j = \frac{\sum_{k=1}^j \Delta\theta_k \sum_{n=0}^{\infty} G_n \exp\left[-\frac{2\lambda_n^2}{Pe_f}(X - (k-1)\Delta X)\right]}{2 \sum_{k=1}^j \Delta\theta_k \sum_{n=0}^{\infty} \frac{G_n}{\lambda_n^2} \exp\left[-\frac{2\lambda_n^2}{Pe_f}(X - (k-1)\Delta X)\right]}. \quad (2)$$

where $\Delta\theta_k = (\theta_{Ri})_k - (\theta_{Ri})_{k-1}$ and $j = \text{int}\left(\frac{X}{\Delta X}\right) + 1$. The values of constant G_n and eigenvalues λ_n can be found in the studies of [20]. Furthermore, for turbulent flow, the local

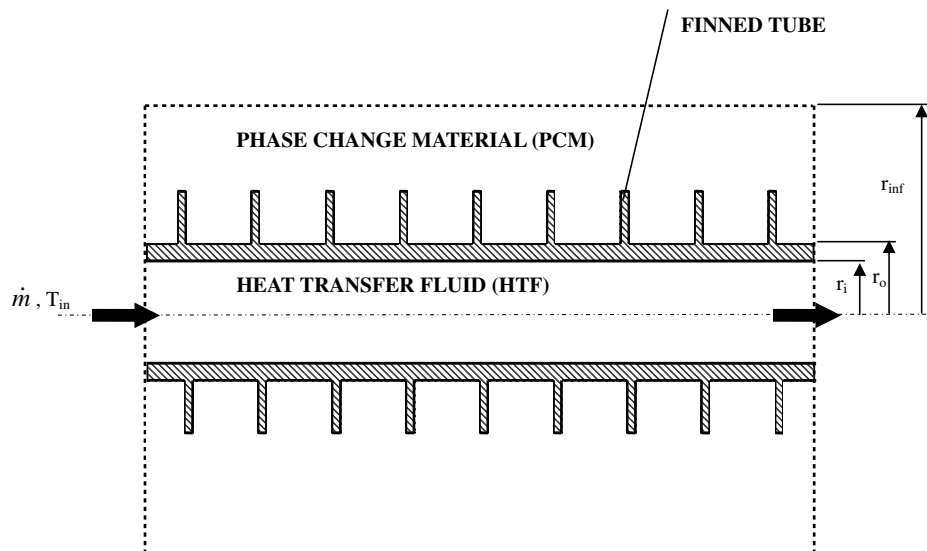


Fig. 2. A sectional view of the finned tube.

Nusselt number can be obtained by using empirical correlation described by [22].

For finned pipe wall, the energy equation is well known as the two-dimensional heat conduction equation,

$$\frac{\partial \theta}{\partial \tau} = \frac{\alpha_f}{\alpha_r} \left[\frac{1}{R} \frac{\partial}{\partial R} \left(KR \frac{\partial \theta}{\partial R} \right) + \frac{\partial}{\partial X} \left(K \frac{\partial \theta}{\partial X} \right) \right]. \quad (3)$$

As the initial temperature of the system is considered to be at a same or close to the phase change temperature, the natural convection effect around the tube and fins can be neglected. The heat conduction in the PCM is described by a temperature transforming method using a fixed grid numerical model [5]. This model assumes that solidification process occurs over a range of phase change temperature from $T_m - \delta T_m$ to $T_m + \delta T_m$, but it can also be successfully used to simulate solidification process occurring at a single temperature by taking a small range of phase change temperature, $2\delta T_m$. The dimensionless heat transfer equation for the PCM is written as

$$\frac{\partial(C\theta)}{\partial \tau} = \frac{\alpha_1}{\alpha_f} \left(\frac{1}{R} \frac{\partial}{\partial R} \left(KR \frac{\partial \theta}{\partial R} \right) + \frac{\partial}{\partial X} \left(K \frac{\partial \theta}{\partial X} \right) \right) - \frac{\partial S}{\partial \tau}, \quad (4)$$

where

$$C = C(\theta) = \begin{cases} C_{sl} & \theta < -\delta\theta_m & \text{solid phase} \\ \left(\frac{1}{2}(1 + C_{sl}) + \frac{1}{2\delta\theta_m} \theta \right) & -\theta\delta_m \leq \theta \leq \theta\delta_m & \text{mushy phase} \\ 1 & \theta > \theta\delta_m & \text{liquid phase} \end{cases} \quad (5)$$

$$S = S(\theta) = \begin{cases} C_{sl}\delta\theta_m & \theta < -\delta\theta_m & \text{solid phase} \\ \left(\frac{1}{2}\delta\theta_m(1 + C_{sl}) + \frac{1}{2\delta\theta_m} \theta \right) & -\theta\delta_m \leq \theta \leq \theta\delta_m & \text{mushy phase} \\ C_{sl}\delta\theta_m + \frac{1}{\delta\theta_m} \theta & \theta > \theta\delta_m & \text{liquid phase} \end{cases} \quad (6)$$

$K = K(\theta)$

$$= \begin{cases} K_{sl} & \theta < -\delta\theta_m & \text{solid phase} \\ K_{sl} + (1 - K_{sl})(\theta + \delta\theta_m)/2\delta\theta_m & -\theta\delta_m \leq \theta \leq \theta\delta_m & \text{mushy phase} \\ 1 & \theta > \theta\delta_m & \text{liquid phase} \end{cases} \quad (7)$$

The initial and boundary conditions are defined as follows:

- Initial conditions ($\tau = 0$):

$$0 \leq X \leq L/D, \quad 0 \leq R \leq R_{inf} \theta = \theta_i \quad (8a)$$

- Boundary conditions ($\tau > 0$):

$$X = 0, \quad 0 < R < 0.5: \quad \theta = \theta_{in} = -1, \quad (8b)$$

$$X = 0, \quad 0.5 < R < R_{inf}: \quad \frac{\partial \theta}{\partial X} = 0, \quad (8c)$$

$$0 \leq X \leq L/D, \quad R = R_{inf} \quad \left. \frac{\partial \theta}{\partial R} \right|_{R=R_{inf}} = 0, \quad (8d)$$

$$X = L/D, \quad 0 < R < R_{inf}: \quad \frac{\partial \theta}{\partial X} = 0. \quad (8e)$$

The temperature distribution inside the solution domain is obtained by solving the above listed equations through a control volume approach as introduced by [23]. Assuming

the bulk temperature approach in the pipe flow, the local Nusselt number is determined using Eq. (2) for laminar flow or an empirical correlation for turbulent flow. However, thermal conductivity, K , is calculated by harmonic mean method at the control surface. Semi implicit solver, [24], is used for solving the discretization equations of energy equations. Using this solver, the CPU time is reduced a great amount for a single iteration since this solver requires less heat storage than the other solvers.

Since heat transfer equation occupied by PCM is a non-linear heat conduction equation, iterations are needed for each time step. For a given time step, convergence is declared at the $k + 1$ th iteration when $|\theta_{ij}^{k+1} - \theta_{ij}^k| \leq 10^{-5}$. The numerical results are then verified by testing the resulting predictions for independence of the grid size, time-step and the other parameters. The grid size used for the solution was 168(axial) \times 114(radial) with a time step $\Delta\tau = 0.001$ for finned tube type 2. The total number of axial nodes increases with the number of fins. In addition, starting the fin-tip in PCM, non-uniform grid size is used with a successive ratio of 1.04. Also, the overall heat transfer balance is checked during the calculation process to verify the numerical results. At a time step, the change of heat storage in PCM and finned tube must be equal to the total energy supplied by the heat transfer fluid as follows:

$$\int_0^\tau \frac{\pi}{4} \cdot Pe_f \cdot C_f \cdot (\theta_{b,out} + 1) \cdot d\tau = \int_0^L \int_{R_i}^{R_{out}} 2\pi \cdot R \cdot (H - H_i) \cdot dR \cdot dX, \quad (9)$$

where $H = CT + S$ stands for the total enthalpy at the control volume. The left side of the equation represents the thermal energy supplied by the heat transfer fluid whereas the right side of the equation represents the thermal stored energy in the PCM and finned tube. The difference between the two sides is found to be less than 2% by Ereke et al. [12].

4. Artificial neural network (ANN) approach

In the ANN approach, neuron is a basic processor in neural networks. Each neuron has one output, based on the situation of the neuron activation, and can receive many inputs from other neurons. Artificial neurons are modeled as a multi-input non-linear process with weighted interconnections. The back-propagation algorithm is considered to be the most suitable method for training multi-layer feed-forward networks as suggested by many [25–28] and summarized as follows:

1. Present a training pattern and propagate it through the network to obtain the outputs.
2. Initialization: Initialize all weights to small random values and threshold values. Set all weights and threshold to small random values. Usually the training sets are normalized to the values between -0.9 and 0.9 during processing.

3. Calculate the net input to the j th node in the hidden layer

$$\text{net}_j = \sum_{i=1}^n w_{ij}x_i - \theta_j, \quad (10)$$

where i is the input node, j hidden layer node, x is the input, w_{ij} weights value connection from the i th input node to the j th hidden layer node and θ_j is the threshold between the input and hidden layers.

4. Calculate the output of the j th node in the hidden layer:

$$h_j = f_h \left(\sum_{i=1}^n w_{ij}x_i - \theta_j \right), \quad (11)$$

$$f_h(x) = \frac{1}{1 + e^{-\lambda_h x}}, \quad (12)$$

where h_j is the vector of hidden-layer neurons, $f_h(\cdot)$ is a logistic sigmoid activation function from input layer to hidden layer, and λ_h is variable which controls the slope of the sigmoidal function.

5. Calculate the net input to the k th node in the hidden layer:

$$\text{net}_k = \sum_j w_{kj}x_j - \theta_k, \quad (13)$$

where k is represents the output layer, w_{kj} is the weights connection from the j th hidden layer node to the k th output layer and θ_k is the threshold connecting the hidden and output layers.

6. Calculate the output of the k th node in the output layer:

$$y_k = f_k \left(\sum_j w_{kj}x_j - \theta_k \right), \quad (14)$$

$$f_k(x) = \frac{1}{1 + e^{-\lambda_k x}}, \quad (15)$$

where y_k is the output of output-layer neurons, $f_k(\cdot)$ is a logistic sigmoid activation function from hidden layer to output layer and λ_k is variable which controls the slope of the sigmoid functional.

7. Calculate errors: The output layer the errors between the target and the observed output is:

$$\delta_k = -(d_k - y_k)f'_k \quad (16)$$

$$f'_k = y_k(1 - y_k) \text{ for sigmoid function,}$$

where δ_k is the vector of errors for each output neuron and d_k is the target activation of output layer. δ_k depends only on the error $(d_k - y_k)$ and f'_k is the local slope of the node activation function for output nodes. The hidden layer error becomes

$$\delta_j = f'_h \sum_{k=1}^n w_{kj}\delta_k \quad (17)$$

$$f'_h = h_j(1 - h_j) \text{ for sigmoid function,}$$

where δ_j is the vector of errors for each hidden layer neuron. δ_j is a weighted sum of the all nodes and f'_h is

the local slope of the node activation function for hidden nodes.

8. Adjust the weights and thresholds in the output layer:

$$w_{kj}^{(t+1)} = w_{kj}^{(t)} + \alpha\delta_k h_j + \eta(w_{kj}^{(t)} - w_{kj}^{(t-1)}), \quad (18)$$

$$\theta_K^{t+1} = \theta_K^{(t)} + \alpha\delta_k, \quad (19)$$

where α is the learning rate, η is the momentum factor and t is time period. The learning rate and the momentum factor are used to allow the previous weight change to influence the weight change in this time period, t . These calculation steps repeat until the output layer error is within desired tolerance for each pattern and neuron.

5. Results and discussion

The feed-forward neural network has become the most popular among the various types of a neural network for various applications, and the back-propagation network is the most common technique for feed forward neural network since there is a mathematically strict learning scheme to train the network and guarantee mapping between inputs and outputs. In this study, an ANN modeling for prediction of the amount of heat transfers in heat storage through PCM around the finned tube is performed. In this regard, a feed-forward back-propagation is used for the training and learning processes. A computer code in the C++ programming language is developed to solve the ANN model algorithm. Neural networks need a range of input and output values which should be between 0.1 and 0.9 to the restriction of sigmoid function. Experimental data and required data are normalized in order to use the values in this study through

$$\frac{\text{Actual data} - \text{Minimum data}}{\text{Maximum data} - \text{Minimum data}} \times (\text{High data} - \text{Low data}) + \text{Low data}, \quad (20)$$

where minimum refers to the annual minimum data value, maximum to the annual maximum data value, high to the

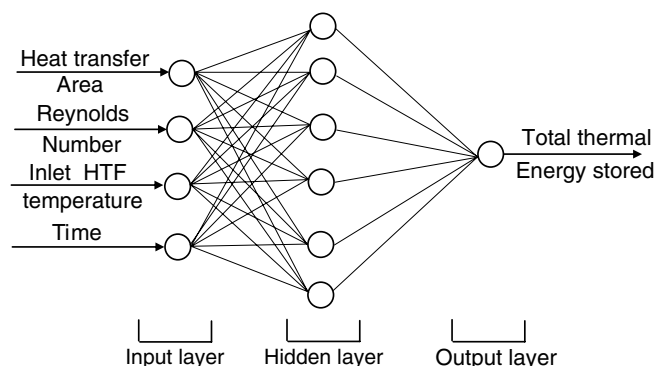


Fig. 3. A three-layer feed-forward back-propagation neural network for heat transfer analysis.

Table 2

Prediction errors associated with the ANN configuration for stored thermal energy in the learning process

# of neurons in hidden layer	AMRE (%)	STD (%)	R^2
8	6.7181	7.8695	0.9917
13	6.6384	7.7835	0.9919
18	6.6562	8.0609	0.9918

maximum normalized data value = 0.9, and low to the minimum normalized data value to be 0.1 as commonly preferred, e.g., [29].

A three-layer feed-forward back-propagation neural network for heat storage is performed as shown Fig. 3. There

were four network input parameters as heat transfer area, Reynolds number, inlet temperature of heat transfer fluid, and time. The output term was the stored thermal energy. The weights, biases and hidden node numbers are altered to minimize the error between the output values and the current data. In order to obtain the least error convergence, the configurations of the ANN are set by selecting the number of hidden layers and nodes, and the learning rate and momentum coefficient. The 240 cases formed out of experimental data set are divided two data set groups, such as that first data group consists of 200 sets to be used for trainings of the network (83% of all data) and the other data group has 40 cases to be used to verify of the ANN model that selected

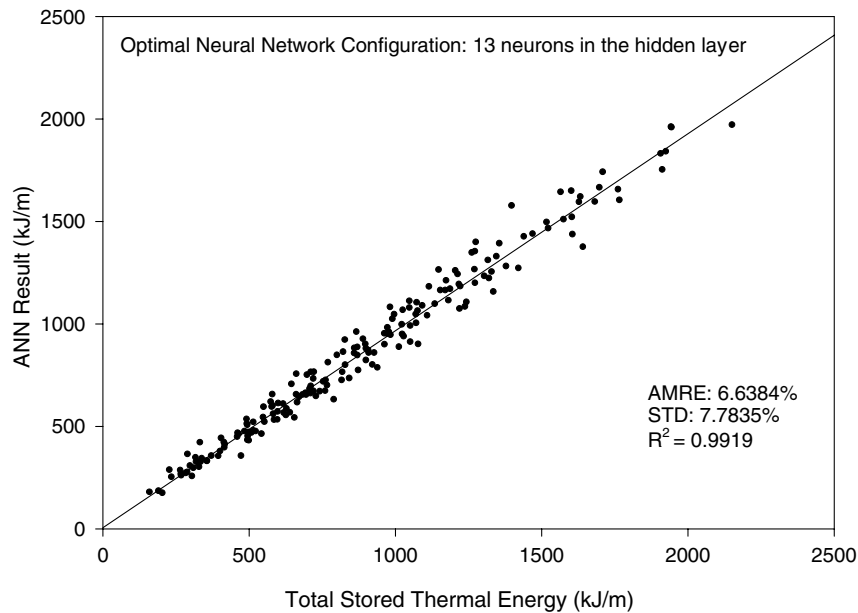


Fig. 4. Comparison of predicted and desired output values for the stored thermal energy.

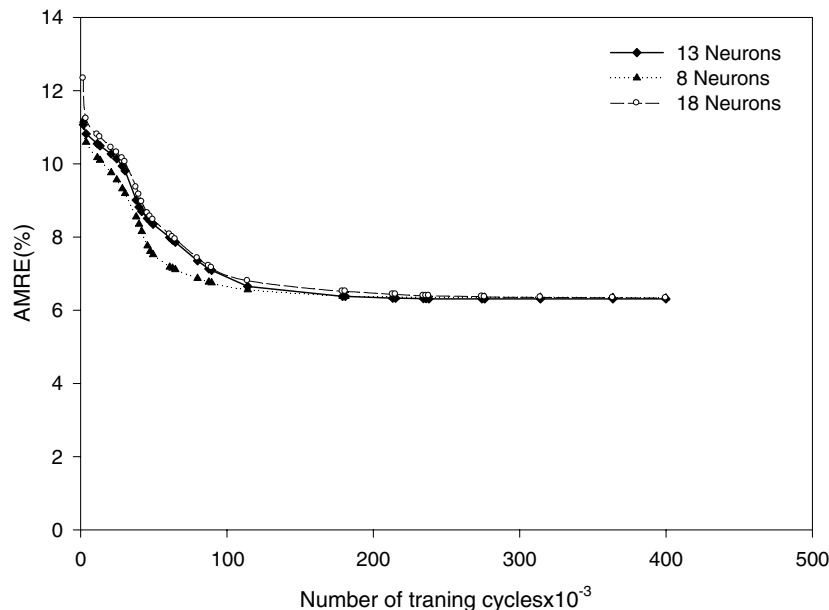


Fig. 5. The network performance with various neuron numbers in the hidden layer.

Table 3
Total stored energy values predicted by the ANN model and numerical model at various experimental conditions for tube type 2

Experimental conditions (Reynolds number, inlet temperature and time)		Total stored energy (kJ/m)								
		Experimental results	Numerical model				ANN Model			
			Results	AMRE (%)	STD	R^2	Results	AMRE (%)	STD	R^2
<i>Re</i> = 500										
−10 °C	30 min	184.72	183.13	0.86	0.02646	0.9999	174.93	5.30	0.00477	0.9972
	60 min	348.28	349.15	0.25	0.02442	1.0000	326.61	6.22	0.00624	0.9961
	90 min	496.21	505.22	1.82	0.02157	0.9997	454.48	8.41	0.00975	0.9929
	120 min	644.92	654.10	1.42	0.02229	0.9998	557.67	13.53	0.01795	0.9817
−15 °C	30 min	281.03	267.98	4.64	0.03336	0.9978	255.76	8.99	0.01068	0.9919
	60 min	533.82	506.09	5.19	0.03437	0.9973	468.27	12.28	0.01595	0.9849
	90 min	770.76	727.77	5.58	0.03507	0.9969	650.29	15.63	0.02131	0.9756
	120 min	971.42	938.28	3.41	0.03111	0.9988	796.08	18.05	0.02519	0.9674
−20 °C	30 min	346.69	340.94	1.66	0.02791	0.9997	328.45	5.26	0.00471	0.9972
	60 min	664.86	639.45	3.82	0.03186	0.9985	607.28	8.66	0.01015	0.9925
	90 min	928.16	915.99	1.31	0.02728	0.9998	866.35	6.66	0.00695	0.9956
	120 min	1187.49	1178.18	0.78	0.02632	0.9999	1092.37	8.01	0.00911	0.9936
<i>Re</i> = 1000										
−15 °C	30 min	275.53	321.12	16.54	0.00532	0.9726	279.67	1.50	0.00612	0.9998
	60 min	531.71	597.38	12.35	0.00233	0.9847	515.91	2.97	0.00104	0.9991
	90 min	762.73	850.74	11.54	0.00382	0.9867	719.56	5.66	0.00535	0.9968
	120 min	966.93	1089.26	12.65	0.00179	0.9840	886.39	8.33	0.00962	0.9931
<i>Re</i> = 2000										
−15 °C	30 min	312.89	372.40	19.02	0.00984	0.9638	334.69	6.97	0.01488	0.9951
	60 min	590.57	682.67	15.60	0.00359	0.9757	609.05	3.13	0.00873	0.9990
	90 min	843.77	963.42	14.18	0.00101	0.9799	850.18	0.76	0.00493	0.9999
	120 min	1063.06	1225.94	15.32	0.00309	0.9765	1053.49	0.90	0.00227	0.9999
<i>Re</i> = 3000										
−15 °C	30 min	416.75	478.83	14.90	0.00231	0.9778	397.67	4.58	0.00362	0.9979
	60 min	730.25	831.83	13.91	0.00051	0.9806	698.33	4.37	0.00328	0.9981
	90 min	1018.75	1139.24	11.83	0.00329	0.9860	965.57	5.22	0.00464	0.9973
	120 min	1281.75	1421.37	10.89	0.00500	0.9881	1195.62	6.72	0.00705	0.9955
<i>Re</i> = 5000										
−10 °C	30 min	319.40	461.56	44.51	0.05638	0.8019	357.72	12.00	0.02293	0.9856
	60 min	570.66	770.15	34.96	0.03894	0.8778	620.70	8.77	0.01776	0.9923
	90 min	789.07	1035.13	31.18	0.03205	0.9028	849.99	7.72	0.01608	0.9940
	120 min	984.29	1272.47	29.28	0.02857	0.9143	1054.57	7.14	0.01515	0.9949
−15 °C	30 min	472.04	619.36	31.21	0.03209	0.9026	486.44	3.05	0.00860	0.9991
	60 min	818.17	1030.59	25.96	0.02252	0.9326	831.43	1.62	0.00631	0.9997
	90 min	1132.52	1380.66	21.91	0.01512	0.9520	1132.18	0.03	0.00367	1.0000
	120 min	1402.43	1699.08	21.15	0.01373	0.9553	1389.67	0.91	0.00226	0.9999
−20 °C	30 min	608.69	752.89	23.69	0.01837	0.9439	613.74	0.83	0.00504	0.9999
	60 min	1035.99	1246.88	20.36	0.01228	0.9586	1050.49	1.40	0.00596	0.9998
	90 min	1423.98	1671.69	17.40	0.00687	0.9697	1436.37	0.87	0.00511	0.9999
	120 min	1758.65	2057.08	16.97	0.00610	0.9712	1741.06	1.00	0.00211	0.9999
<i>Re</i> = 7000										
−15 °C	30 min	553.10	688.11	24.41	0.01968	0.9404	578.88	4.66	0.01118	0.9978
	60 min	927.21	1121.72	20.98	0.01342	0.9560	956.41	3.15	0.00876	0.9990
	90 min	1254.21	1488.61	18.69	0.00924	0.9651	1275.41	1.69	0.00642	0.9997
	120 min	1548.99	1821.52	17.59	0.00724	0.9690	1543.57	0.35	0.00315	1.0000
Average				14.99	0.01791	0.9664		5.58	0.00887	0.9950

randomly 2nd of tube type from the experimental tubes. The learning process is performed using 1st, 3rd, 4th, 5th, 6th, 7th and bare types of tube as shown in Table 1.

The ANN model is now utilized for stored thermal energy by using the four inputs, one output and three different nodes which are 8, 13 and 18 in the hidden layer. In the algorithm, the learning rates and momentum coefficients

are 0.6 for learning processes, in which 400 000 iterations are used to obtain good fits. The three error measuring parameters used to compare the performance of the various ANN configurations as consistent with [30].

The performance of various ANN configurations is compared using the absolute mean relative error (AMRE),

the standard deviations in the relative (STD) errors and the absolute fraction of variance (R^2) in Table 2 through the following equations:

$$AMRE = \frac{1}{n} \sum_{i=1}^n ABS(B), \tag{21}$$

$$STD = \sqrt{\frac{\sum_{i=1}^n (B - \bar{B})^2}{n - 1}}, \tag{22}$$

$$R^2 = 1 - \left[\frac{\sum_{i=1}^n (y_i - a_i)^2}{\sum_{i=1}^n (a_i)^2} \right], \tag{23}$$

where y_i is the prediction value, a_i is the experimental value, n is the number of data values and $B = (y_i - a_i)/a_i$.

Also, Table 2 lists the associated prediction errors, the absolute mean relative error (AMRE), the standard deviations in the relative (STD) errors and the absolute fraction of variance R^2 with ANN configurations for stored thermal energy in the learning process including of 200 experimental data for training data set. The 13 nodes of hidden configuration appeared to be the best selection due to the results of prediction errors from Table 2. Fig. 4 shows a plot of the predicted versus desired output values of the

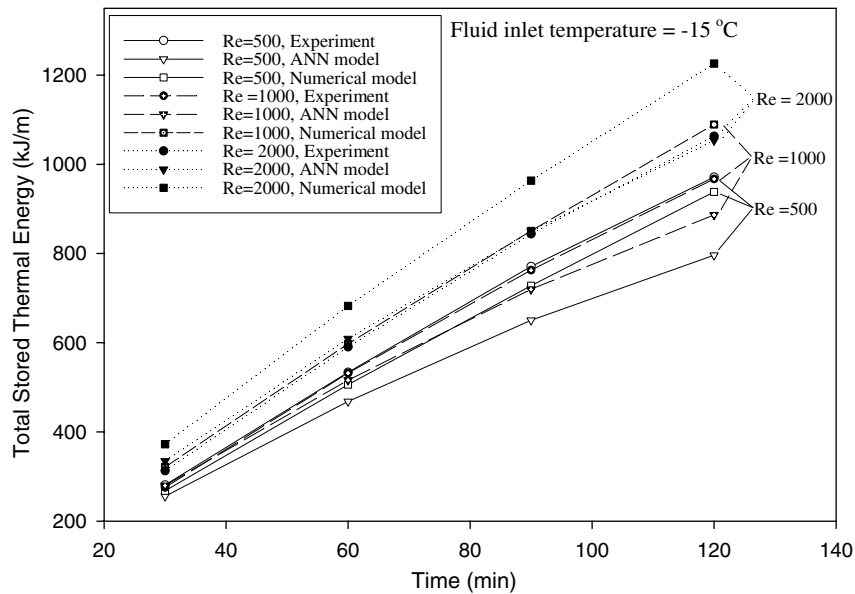


Fig. 6. Comparison of the results of the ANN model with numerical model results and experimental data at $Re = 500, 1000$ and 2000 and an inlet temperature of HTF of $-15\text{ }^\circ\text{C}$.

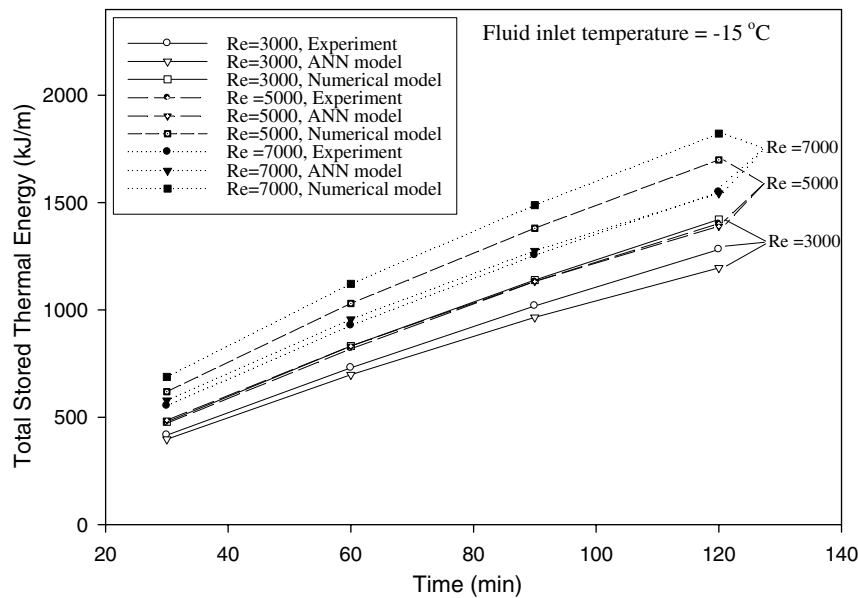


Fig. 7. Comparison of the results of the ANN model with numerical model results and experimental data at $Re = 3000, 5000$ and 7000 and an inlet temperature of HTF of $-15\text{ }^\circ\text{C}$.

Table 4
Comparison of average AMREs between the ANN approach and the numerical model for the tube type 2 at different Reynolds number at an inlet temperature HTF of $-15\text{ }^{\circ}\text{C}$

Average AMRE (%)	Reynolds number					
	500	1000	2000	3000	5000	7000
ANN model	13.74	4.62	2.94	5.22	1.40	2.46
Numerical model	4.71	13.27	16.03	12.88	25.06	20.42

stored thermal energy using the optimal neural network in the learning process.

The network performance with various neuron numbers in the hidden layer is presented in Fig. 5. As seen in the figure, the optimum neurons numbers are 13 neurons in the hidden layer for 400000 iteration cycles. The ANN results are then compared with the experimental and numerical results for total stored thermal energy in the tube type-2 for various experimental conditions in Table 3. For comparison purposes of ANN model and the numerical model, 13 of hidden number, 0.6 of the learning rates and momentum coefficients are used in the model. The results of this using the absolute mean relative error (AMRE), the standard deviations in the relative (STD) errors and the abso-

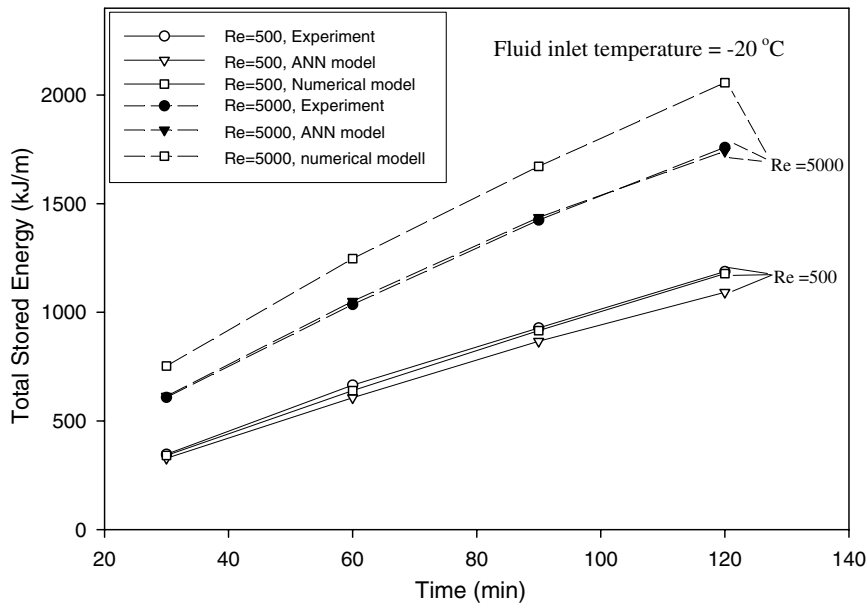


Fig. 8. Comparison of the results of the ANN model with numerical model results and experimental data at $Re = 500$ and 5000 and an inlet temperature of HTF of $-20\text{ }^{\circ}\text{C}$.

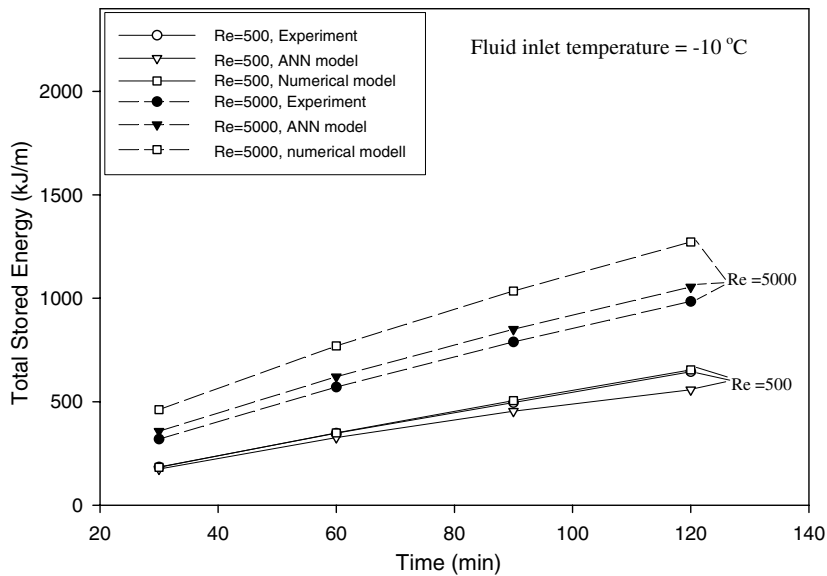


Fig. 9. Comparison of the results of the ANN model with numerical model results and experimental data at $Re = 500$ and 5000 and an inlet temperature of HTF of $-10\text{ }^{\circ}\text{C}$.

lute fraction of variance R^2 are employed for comparing each other. The ANN model has an average AMRE of 5.58%, an average STD of 0.00887 and an average R^2 of 0.9950, respectively while the numerical one has the values of 14.99%, 0.01791 and 0.9664 for the same parameters.

The comparisons between the ANN model and the numerical model along with the experimental data for the total stored thermal energy at $Re = 500, 1000$ and 2000 are shown in Fig. 6, for the Re values of $3000, 5000$ and 7000 in Fig. 7 at an inlet temperature of

Table 5

Total stored energy values predicted by both linear and polynomial (non-linear) equations at various experimental conditions for tube type 2

Experimental conditions (Reynolds number, inlet temperature and time)		Total stored energy (kJ/m)							
		Linear equation ^a				Polynomial equation ^b			
		Results	AMRE (%)	STD	R^2	Results	AMRE (%)	STD	R^2
$Re = 500$									
-10 °C	30 min	36.94	80.00	0.13106	0.3600	174.93	80.17	0.13011	0.3573
	60 min	318.71	8.49	0.01655	0.9928	326.61	42.90	0.07043	0.8160
	90 min	600.48	21.01	0.03069	0.9558	454.48	5.43	0.01043	0.9971
	120 min	882.26	36.80	0.05597	0.8646	557.67	31.46	0.04865	0.9010
-15 °C	30 min	278.38	0.94	0.00446	0.9999	255.76	31.27	0.05181	0.9022
	60 min	560.15	4.93	0.00494	0.9976	468.27	33.43	0.05526	0.8883
	90 min	841.92	9.23	0.01183	0.9915	650.29	18.81	0.03185	0.9646
	120 min	1123.70	15.68	0.02215	0.9754	796.08	3.39	0.00369	0.9989
-20 °C	30 min	519.82	49.94	0.07701	0.7506	328.45	43.62	0.06812	0.8097
	60 min	801.59	20.57	0.02998	0.9577	607.28	0.70	0.00286	1.0000
	90 min	1083.36	16.72	0.02382	0.9720	866.35	0.26	0.00132	1.0000
	120 min	1365.14	14.96	0.02100	0.9776	1092.37	10.24	0.01467	0.9895
$Re = 1000$									
-15 °C	30 min	326.68	18.56	0.02677	0.9655	279.67	12.33	0.02149	0.9848
	60 min	608.45	14.43	0.02016	0.9792	515.91	24.06	0.04026	0.9421
	90 min	890.22	16.72	0.02381	0.9721	719.56	11.61	0.02032	0.9865
	120 min	1172.00	21.21	0.03100	0.9550	886.39	8.88	0.01248	0.9921
$Re = 2000$									
-15 °C	30 min	423.28	35.28	0.05354	0.8755	334.69	8.14	0.01130	0.9934
	60 min	705.05	19.39	0.02809	0.9624	609.05	15.23	0.02613	0.9768
	90 min	986.82	16.95	0.02419	0.9713	850.18	8.62	0.01554	0.9926
	120 min	1268.60	19.33	0.02800	0.9626	1053.49	8.14	0.01130	0.9934
$Re = 3000$									
-15 °C	30 min	519.88	24.74	0.03667	0.9388	397.67	4.42	0.00534	0.9980
	60 min	801.65	9.78	0.01270	0.9904	698.33	18.19	0.03086	0.9669
	90 min	1083.42	6.35	0.00721	0.9960	965.57	14.82	0.02546	0.9781
	120 min	1365.20	6.51	0.00747	0.9958	1195.62	2.76	0.00615	0.9992
$Re = 5000$									
-10 °C	30 min	471.64	47.67	0.07337	0.7728	357.72	47.87	0.07491	0.7709
	60 min	753.41	32.03	0.04833	0.8974	620.70	11.19	0.01618	0.9875
	90 min	1035.18	31.19	0.04699	0.9027	849.99	14.68	0.02177	0.9784
	120 min	1316.96	33.80	0.05116	0.8858	1054.57	30.40	0.04694	0.9076
-15 °C	30 min	713.08	51.06	0.07881	0.7393	486.44	33.21	0.05144	0.8897
	60 min	994.85	21.59	0.03162	0.9534	831.43	3.32	0.00705	0.9989
	90 min	1276.62	12.72	0.01742	0.9838	1132.18	6.28	0.01179	0.9961
	120 min	1558.40	11.12	0.01485	0.9876	1389.67	2.68	0.00255	0.9993
-20 °C	30 min	954.52	56.81	0.08802	0.6772	613.74	53.37	0.08373	0.7151
	60 min	1236.29	19.33	0.02800	0.9626	1050.49	5.78	0.00751	0.9967
	90 min	1518.06	6.61	0.00762	0.9956	1436.37	4.06	0.00823	0.9984
	120 min	1799.84	2.34	0.00079	0.9995	1741.06	0.79	0.00300	0.9999
$Re = 7000$									
-15 °C	30 min	906.28	63.85	0.09929	0.5923	578.88	48.69	0.07623	0.7629
	60 min	1188.05	28.13	0.04209	0.9209	956.41	6.20	0.00818	0.9962
	90 min	1469.82	17.19	0.02457	0.9704	1275.41	0.07	0.00163	1.0000
	120 min	1751.60	13.08	0.01799	0.9829	1543.57	5.46	0.00701	0.9970
Average			23.43	0.03500	0.9146		17.82	0.02868	0.9356

^a Linear equation; $Q_{\text{stored}} = -1054.3570 + 0.0966Re + 9.3924\text{Time} - 8.2888\text{Temperature} + 1687.3365\text{Area}$.

^b Polynomial equation (non-linear); $Q_{\text{stored}} = -151.9903 + 0.0968Re + 0.0601\text{Time}^2 - 0.0659\text{Temperature}^3 + 27374.7856\text{Area}^4$.

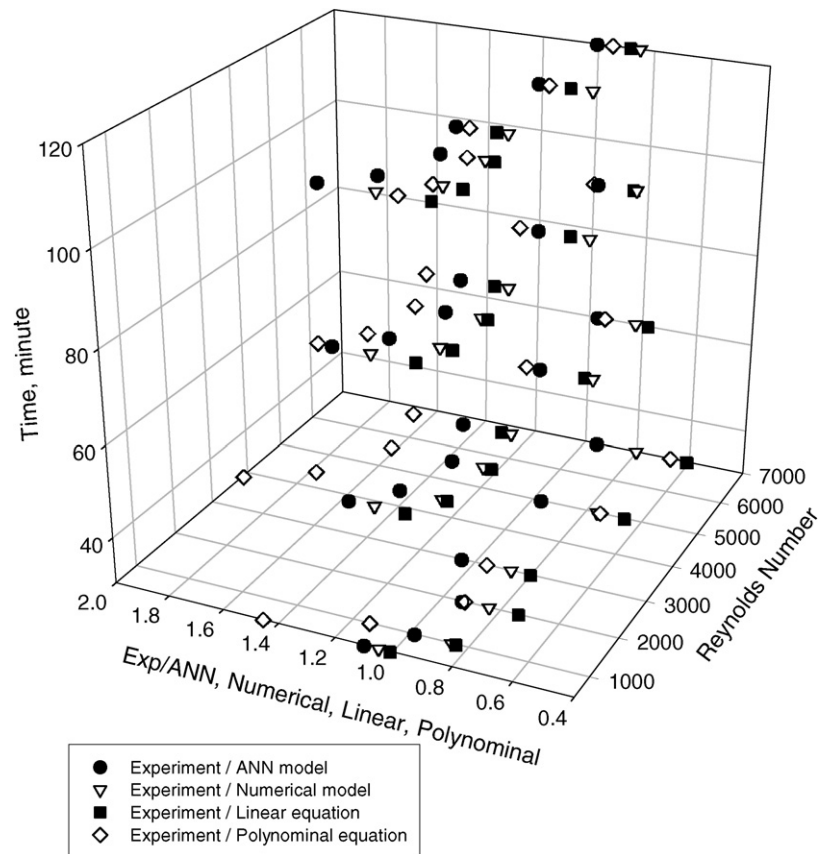


Fig. 10. Comparison of ANN approach, numerical model and linear and polynomial equations with experimental data at various Reynolds number and time.

–15 °C. In these figures, the ANN prediction has an average AMRE of 13.74, compared to the numerical model prediction with 4.71, in comparison with experimental results for a laminar flow regime at $Re = 500$. Table 4 also shows the average AMRE values for comparison purposes between the ANN and the numerical model for the tube type-2 at different Reynolds number at –15 °C of inlet HTF. It basically shows that the ANN gives better results and agreement in comparison with the experimental data since one key reason for this is that ANN uses some experimental data. Also the comparison between the ANN model and the numerical model along with the experimental data for the total stored thermal energy at $Re = 500$ and 5000 at –20 °C inlet temperature of HTF in Fig. 8, and for an inlet temperature of HTF at –10 °C in Fig. 9. Although these figures show that both ANN and numerical model results are close to the experimental data at $Re = 500$, the ANN approach provides better agreement than the numerical model at $Re = 5000$ for both inlet temperatures of HTF.

It is important to note that the ANN can be considered a powerful tool for heat transfer analysis during such two-phase heat transfer processes due to costly and difficult experimental works and measurements. So ANN can easily overcome such problems using the available data for heat transfer predictions.

Here, we validate the ANN model. Note that both linear and polynomial (non-linear) equations are developed through the SigmaPlot using over 240 experimental data as training data for the model. The best fitting equations in linear and non-linear forms are obtained as

$$\begin{aligned} \bullet \quad Q_{\text{stored}} &= -1054.3570 + 0.0966Re + 9.3924\text{Time} \\ &\quad - 8.2888\text{Temperature} + 1687.3365\text{Area} \\ \bullet \quad Q_{\text{stored}} &= -151.9903 + 0.0968Re + 0.0601\text{Time}^2 \\ &\quad - 0.0659\text{Temperature}^3 + 27374.7856\text{Area}^4 \end{aligned}$$

These equations are used to validate the ANN model for the second tube as summarized in Table 5 and Fig. 10. These clearly show that ANN provides better agreement, as expected, with the experimental data. An uncertainty analysis is included in training and test data groups for this study.

6. Conclusions

In this paper we have applied a feed-forward back-propagation artificial neural network (ANN) algorithm for heat transfer analysis of phase change process in a latent heat thermal energy storage system with finned tube. We also verify the present ANN model through comparisons with the numerical results and experimental data and find out that the ANN model provides better agreement for both

laminar and turbulent flows in heat storage system with the experimental data, compared to the numerical model results, since the ANN model employs some experimental data. Furthermore, the ANN model has an average AMRE of 5.58 while numerical model ends up 14.99. The results show that ANN approach appears to be promising tool for thermal analysis of both latent and sensible thermal energy storage systems.

Acknowledgements

The authors acknowledge the support provided by their universities and the Natural Sciences and Engineering Research Council of Canada in Canada.

References

- [1] I. Dincer, A. Dost, A perspective on thermal energy storage systems for solar energy applications, *Int. J. Energy Res.* 20 (1996) 547–557.
- [2] I. Dincer, M.A. Rosen, Energetic, environmental and economic aspects of thermal energy storage systems for cooling capacity, *Appl. Therm. Eng.* 21 (2001) 1105–1117.
- [3] I. Dincer, M.A. Rosen, *Thermal Energy Storage Systems and Applications*, John Wiley and Sons, London, 2002.
- [4] I. Kar, C.L.F. Alves, Analysis of the shell-and-tube PCM storage system, *Proceedings of the 8th International Heat Transfer Conference* (1986) 1781–1786.
- [5] Y. Cao, A. Faghri, Performance characteristics of a thermal energy storage module: a transient PCM/forced convection conjugate analysis, *Int. J. Heat Mass Transfer* 34 (1991) 93–101.
- [6] Y. Cao, A. Faghri, A PCM/forced convection conjugate transient analysis of energy storage systems with annular and countercurrent flows, *ASME J. Heat Transfer* 113 (1991) 37–42.
- [7] A.G. Bathelt, R. Viskanta, Heat transfer and interface motion during melting and solidification around a finned horizontal sink/source, *J. Heat Transfer* 103 (1981) 720–726.
- [8] K. Sasaguchi, Y. Sakamoto, Effects of natural convection on melting of a phase change material around a finned tube, *Trans. JSME* 55 (513) (1989) 1418–1425.
- [9] P.V. Padmanabhan, M.V. Khrishna, Outward phase change in a cylindrical annulus with axial fins on the inner tube, *Int. J. Heat Mass Transfer* 29 (1989) 1855–1868.
- [10] M. Lacroix, Study of the heat transfer behaviour of a latent heat thermal energy storage unit with a finned tube, *Int. J. Heat Mass Transfer* 36 (1993) 2083–2092.
- [11] Y. Zhang, A. Faghri, Analytical solution of thermal energy storage system with conjugate laminar forced convection, *Int. J. Heat Mass Transfer* 39 (1996) 717–724.
- [12] A. Ereğ, Z. Ilken, M.A. Acar, Experimental and numerical investigation of thermal energy storage with a finned tube, *Int. J. Energy Res.* 29 (2005) 283–301.
- [13] D. Darrell, Massie, Optimization of a building's cooling plant for operating cost and energy use, *Int. J. Therm. Sci.* 41 (2002) 1121–1129.
- [14] J. Yang, H. Rivard, R. Zmeureanu, On-line building energy prediction using adaptive artificial neural networks, *Energy Build.* 37 (2005) 1250–1259.
- [15] A.E. Ben-Nakhi, M.A. Mahmoud, Cooling load prediction for buildings using general regression neural networks, *Energy Convers. Manage.* 45 (2004) 2127–2141.
- [16] A. Abbassi, L. Bahar, Application of neural network for the modeling and control of evaporative condenser cooling load, *Appl. Therm. Eng.* 25 (2005) 176–186.
- [17] S. Lecoeuche, T.S. Lalot, B. Desmet, Modelling a non-stationary single tube heat exchanger using multiple coupled local neural networks, *Int. Commun. Heat Mass Transfer* 32 (2005) 913–922.
- [18] G. Diaz, M. Sen, K.T. Yang, R.L. McClain, Dynamic prediction and control of heat exchangers using artificial neural networks, *Int. J. Heat Mass Transfer* 44 (2001) 1671–1679.
- [19] A. Pacheco-Vega, M. Sen, K.T. Yang, R.L. McClain, Neural network analysis of fin-tube refrigerating heat exchanger with limited experimental data, *Int. J. Heat Mass Transfer* 44 (2001) 763–770.
- [20] W.M. Kays, M.E. Crawford, *Convective Heat and Mass Transfer*, McGraw-Hill, New York, 1980.
- [21] Y. Zhang, A. Faghri, Heat transfer enhancement in latent heat thermal energy storage system by using the internally finned tube, *Int. J. Heat Mass Transfer* 39 (1996) 3165–3173.
- [22] V. Gnielinski, New equations for heat and mass transfer in turbulent pipe and channel flow, *Int. Chem. Eng.* 16 (1976) 359–368.
- [23] S.V. Patankar, *Numerical Heat Transfer and Fluid Flow*, McGraw-Hill, New York, 1980.
- [24] S.L. Lee, A strongly implicit solver for two-dimensional elliptic differential equations, *Numer. Heat Transfer* 16 (B) (1989) 161–178.
- [25] R.D. Reed, R.J. Marks, *Neural Smoothing: Supervised Learning in Feedforward Artificial Neural Networks*, MIT Press, London, 1999.
- [26] R. Rojas, *Neural Networks*, Springer-Verlag, Berlin, 1996.
- [27] S. Haykin, *Neural Networks: A Comprehensive Foundation*, Prentice Hall, New Jersey, 1999.
- [28] L. Fausett, *Fundamentals of Neural Networks: Architecture Algorithms and Applications*, Prentice Hall, Englewood Cliffs, NJ, 1994.
- [29] G.E. Nasr, E.A. Badr, C. Joun, Backpropagation neural networks for modeling gasoline consumption, *Energy Convers. Manage.* 44 (2003) 893–905.
- [30] S.S. Sablani, A. Kacimov, J. Perret, A.S. Mujumdar, A. Campo, Non-iterative estimation of heat transfer coefficients using artificial neural network models, *Int. J. Heat Mass Transfer* 48 (2005) 665–679.